We would like to express gratitude to the Referees for the detailed and precise analysis of our manuscript that contributes towards its improvement. We have taken all of the comments into account in the revision (changes appear in red type) and explain this in detail in the following sections.

1 Technical comments from Reviewer 1

Question 1: In the work, the symbol V has two different meanings. One is the volume in Figure 1, the other is the potential function on Page 5.

Answer: The volume of the compartments in Figure 1 was designated as V_c.

Question 2: In stochastic differential equation (9), you can add the initial condition $Y_0 = y_0$. On the second line from the bottom of Page 7, the generator should be $Au = \lim_{t\to 0} \frac{\mathbb{E}u(y_t)-u(y_0)}{t}$.

Answer: The initial condition $Y_0 = y_0$ is added to the equation (9). The generator on line 165 is corrected as suggested.

Question 3: In the manuscript, the authors adopted the αstable non-Gaussian Lévy noise to model the extreme events? Can you give the comparison between the Brownian motion and Lévy flight?

Answer: We compare the processes in the end of the section 2.1.1.

Question 4: In equation (14), what is the definition of I?

Answer: The definition of indicator function I is given by equation (15).

Question 5: In Section 2.1.5, what is the definition of $p_i(y), m, M$? Could you represent the definition of stochastic basin of attraction to the one-dimensional case since that the escape boundary only has two direction in the one-dimension. The work "Y. Zheng, L. Serdukova, J. Duan, J. Kurths, Transitions in a genetic transcriptional regulatory system under Lévy motion, Sci. Rep. 6 (2016) 29274." also introduces the stochastic basin of attraction, which can be added to the references.

Answer: In Section 2.1.5 the definition of stochastic basin of attraction is adapted to the one-dimensional case and the measures of m and M are specified. The work of Y. Zheng is added to the references line 355.

Question 6: In the manuscript, the authors show the three concepts, mean residence time, first passage probability and stochastic basin of attraction to perform the stability analysis. Could you show us how to solve the non local equations (14) (15) and (17)?

Answer: At the end of section 2.1.3 we describe the numerical method that we use to solve these equations.

2 Technical comments from Reviewer 2

Question 1: Title: The model does not represent the global thermohaline circulation but the Atlantic MOC.

Answer: We have made proposed amendments to both the title and the text.

Question 2: l17: Tides are no part of the THC. l27: There is no surplus of precipitation over evaporation at low latitudes, except in a small zone near the equator (ITCZ).

Answer: The suggested changes are introduced in the lines 16 and 26.

Question 3:There should be a justification that the variability in the freshwater forcing can be represented by an α-stable process. Here, the time scale considered is important: when focus is on Dansgaard-Oeschger (DO) events (e.g. Ditlevsen 1999), this is a different issue that when the stability of the present-day MOC is considered. As for the latter case, many observations and model results (reanalyses, CMIP6) are available for justification.

Answer: We consult the publications (bibliography line 372) and introduce the suggested justification on lines 55-60.

Question 4: The new aspects in this paper, in relation to the one just published (Tesfay et al., 2020 in the reference list), should be clarified as the same model and same noise are investigated.

Answer: This clarification is included on page 3 in the first paragraph.

Question 5: l72: $\Delta\rho$ should be divided by ρ_0. l99: β is no restoration "tensility" but a ratio of a diffusive and a restoring time scale. l101: definition of μ^2 is wrong. l105, 107: $dt \to d\tau$. l129: the relation between the amplitude of dL_t and F is missing.

Answer: The respective corrections were introduced in the equations (2), (6) and (7).

Question 6: Fig. 6 contains no probability distributions as for each curve the integral is not 1.

Answer: Figure 6 has been replaced according to the suggestion.

Question 7: The methodology in section 2.1 should be better explained and only provide well explained mathematical results with reference to the mathematical details. It appears now to have been copied from a mathematics paper with many symbols unexplained. At line 130, there is a reference to a "Methods" section which is not there.

Answer: All mathematical concepts were described in more detail in section 3, on pages 7, 8 and 9.

Question 8: Section 3: I would suggest to split the results into two sections: (i) DO transitions. Connect the results to the Ditlevsen (1999) analysis and proposed noise structure. Can the α-stable noise better describe the transition behavior (as in the proxy data), than just Brownian noise? (ii) Present-day MOC. Is the transition probability of a MOC transition increased under climate change, when incorporating an α-stable process in the freshwater flux noise?

Answer: To make the proposed comparison (α-stable vs Brownian noise) we should include the parameter $\alpha = 2$ (which corresponds to the Brownian case) in the simulations of stochastic perturbations. We leave this option for future studies.

Question 9: Improve also the interpretation of the results: in the present text, lines 209-210, lines 222-223, lines 267-268 and lines 277-281 make no sense.

Answer: Reading more articles about timescales of AMOC decline, AMOC response to fresh water forcing and stability of AMOC off-state we try to improve the interpretation of the results, see the changes made in the section 4.

Influence of extreme events modeled by Lévy flight on Atlantic meridional overturning circulation stability

Daniel Tesfay[1], Larissa Serdukova[2], Yayun Zheng[1], Pingyuan Wei[1], Jinqiao Duan[3], and Jürgen Kurths[4]

[1]School of Mathematics and Statistics & Wuhan Center for Mathematical Sciences, Huazhong University of Science and Technology, Wuhan 430074, China

[2]Department of Mathematics and Statistics, Reading University, Reading RG6 6AX, UK

[3]Department of Applied Mathematics, Illinois Institute of Technology, 312-567-5335, Chicago 60616, USA

[4]Research Domain on Transdisciplinary Concepts and Methods, Potsdam Institute for Climate Impact Research, PO Box 60 12 03, 14412 Potsdam, Germany

Correspondence: Larissa Serdukova (l.i.serdukova@reading.ac.uk)

Abstract.

How will extreme events due to human activities and climate change affect the Atlantic meridional overturning circulation is a key concern in climate predictions. The stability of the thermohaline circulation with respect to extreme events, such as fresh-water oscillations is examined using a conceptual stochastic Stommel two-compartment model. The extreme fluctuations are modeled by symmetric α-stable Lévy motions whose pathways are cádlág functions with at most a countable number of jumps. The mean first passage time, escape probability and stochastic basin of attraction are used to perform the stability analysis of *on (off)* equilibrium states. Our results argue that for model with weak fresh-water forcing strength, the greatest threat to the stability of the *on*-state represents noise with low jumps and higher frequency that can be seen as freshwater inputs from glacier melting due to ocean warming caused by increased greenhouse gas emissions. On the other hand, the *off*-state stability is more vulnerable to the agitations with moderate jumps and frequencies which can be interpreted as a possible scenario of Atlantic thermohaline circulation recovery. Under the repercussion of stochastic noise, *on* to *off* transitions are more expected in the model with the strong fresh-water influx. Moreover, transitions from one metastable state to another are equiprobable when the fresh-water input induces a symmetric potential well.

1 Introduction

Natural and civilization catalyzed fluctuations in climate have significant impact on the ocean and ocean circulation pattern variations greatly affect climate (Chapman and Shackleton, 1999; Clark et. al., 2002). The thermohaline circulation, known as great ocean conveyor as well, has been declared potentially unstable, whose change could lead to abrupt climate shift on all timescales (Marotzke, 2000). Thermohaline circulation is basically an outcome of the interplay of fresh-water with thermal energy along with the ocean-atmosphere interface and inside the ocean competition of temperature and salinity (Rahmstorf, 2003). This enormous oceanic process has a significant contribution in maintaining the equilibrium of Earth's energy framework by redistributing thermal energy of the order 1.2×10^{15}W northwards in the Atlantic ocean. A large proportion of the meridional overturning circulation (MOC) is usually categorized as thermohaline circulation because MOC takes the lion's share in this heat penetration to the north pole (Ganachaud and Wunsch, 2001; Trenberth and Solomon, 1994). The warm and saltier surface water on interannual and even longer time-scales gets freshened and loses heat to the cold atmosphere. Subsequently, the water descends slightly to the bottom of the Atlantic since it gets denser than the underneath water. The cooled water eventually returns southward as deep current and the warm temperature around the equatorial belt opts for upwelling. Thermohaline circulation is a combination of the floating of deep water currents around the equator and in the southern oceans, the horizontal currents, and the descending and forming of deep water in high latitudes. Climate reconstructions indicate that conveyor belt has indispensable contribution in the climate system transitions from cold to warm or from warm to cold climate states (Rahmstorf, 1995; Bond et.al., 1997; Grootes and Stuiver, 1997). In today's warm climate, the thermohaline circulation state is sensitive to increased fresh-water volume. During global warming, the intensity of the water cycle, especially at high latitudes, increases, and the melting of ice accelerates, the supply of fresh water to the North Atlantic will most likely increase, thereby reducing the density of the surface layer in the MOC sinking area. Thus, it seems likely that the thermohaline circulation will weaken over the coming century. Studying the stability of this oceanic conveyor belt by analyzing the influence of internal and external agitations on its dynamical behavior is increasingly pressing presently.

To study how the Atlantic meridional overturning circulation (AMOC) transports properties latitudinally, a conceptual deterministic two-compartment model was forwarded by Stommel (Stommel, 1961). Shreds of evidence from sea observation and model simulation show that the strength of the thermohaline flow is sensitive to the surface fresh-water flux fluctuation (Jackson and Wood, 2017; Caesar et.al., 2018). Competition between thermal versus saline forcing can lead to a multiple equilibria regime if the relaxation time-scales for the temperature and the salinity are distinct. The thermohaline flow system is bistable, one with strong circulation (analogous with the present set up), and the second state with a very weak flow, when the salinity difference is forced by a prescribed fresh-water flux (Marotzke, 2000). The multistability of AMOC is also verified by results obtained from different numerical models (Broecker, 1987). The deterministic compartment model has been further extended to include noisy thermal and saline forcing oscillations (Huang et. al., 1992; Rahmstorf, 1996; Djikstra, 2005).

Forcing the general ocean circulation model with some particularly large stochastic fresh-water fluctuations is found to trigger pulsation of transport from one stable configuration to the other (Mikolajewicz and Maier-Reimer, 1990). Therefore, the fresh-water budget is the main control parameter of the Atlantic circulation, the oscillations of which lead to the circulation response in the form of a hysteresis curve. There is evidence that after the AMOC crossing a threshold exists a temporary resilience period during which the AMOC could still recover if freshwater inflow ceases (Jackson and Wood, 2017).

The Gaussian noise perturbed thermohaline circulation has been under extensive study. For instance, it was shown in (Vélez-Belchí et. al., 2001) that an increment of 5% of the fresh-water forcing in the ocean circulation could stimulate transitions between a high and low salinity difference metastable states. In a time-dependent compartment model for thermohaline circulation with Brownian motion and moderate noise intensity, hysteresis does not adiabatically follow stationary distribution (Bergund and Gentz, 2002). Meanwhile, the noise forcing climate comprises of a non-Gaussian α-stable Lévy noise component (Fuhrer et. al., 1993; Ditlevsen, 1999). The occurrence more than a dozen of additional Dansgaard-Oeschger (D-O) events that took place during the last glacial period could not have been reproduced by using the continuous perturbation processes. As well modern climate models from the fifth Coupled Model Intercomparison Project (CMIP5) predict abrupt non-linear shifts in subpolar North Atlantic dynamics (Sgubin et. al., 2016). The jumps in those events could better be modeled by Lévy flights (Kuhwald and Pavlyukevich, 2016).

Paleoclimatic data indicate the coincidence of transitions from strong to weak or from weak to strong thermohaline circulation states with the occurrence of extreme climatic variations (Vélez-Belchí et. al., 2001). In our previous work (Tesfay et. al., 2020), we investigated the most probable trajectories of such transitions. The results of this study led us to a number of questions, of how is the overturning circulation stable to abrupt climatic changes? And what parameters of Lévy noise most affect the equilibrium of the AMOC? We also estimate possible scenarios for thermohaline circulation regeneration, analyzing the stability of the *off* state under stochastic fresh-water fluctuations.

We analyze the stability of metastable states of the AMOC model by calculating three quantities, namely, mean first passage (exit) time, first passage (escape) probability and stochastic basin of attraction that carry the dynamical information of the model. In the present form of the AMOC, analyzing the intensity and mechanism of the forcing schemes that could trigger such transitions and studying the stability of strong and weak AMOC equilibrium states is of fundamental importance.

Particularly, we will study the effect of extreme events on the scalar stochastic AMOC model

$$dY_t = -V'(Y_t)dt + dL_t^\alpha \tag{1}$$

by measuring the stability of equilibrium states of the salinity difference process Y_t for various values of (nondimensional) fresh-water forcing and non-Gaussianity parameter α. In Eq. (1), V is a potential function (details are given in Section 2).

The paper is structured as follows. In Section 2, we discuss the simplified conceptual stochastic Stommel two-compartment model for AMOC. A brief introduction of the stability analysis measures is provided in Section 3. Stability analysis of the stochastic overturning circulation system is given and results obtained are presented in Section 4. Our findings are summarized in Section 5.

2 Atlantic meridional overturning circulation model

Thermohaline circulation is an oceanographic phenomena that refers to the movement of ocean waters across both hemispheres and is responsible for the heat transfer and redistribution, acting as a regulator of the global climate. The schematic functioning of AMOC is shown in Fig. 1. The main engine of this circulation is the difference in density between ocean currents $\Delta\rho$, which is determined by the salinity S_e, S_p and the temperature T_e, T_p of the water and can be represented by

$$\Delta\rho = \rho_0[\beta_S(S_e - S_p) - \beta_T(T_e - T_p)], \tag{2}$$

where $\beta_T = 0.17 \times 10^{-3}\,{}^o\,C^{-1}$ is the thermal expansion coefficient and $\beta_S = 0.75 \times 10^{-3}$ psu^{-1} is the haline contraction coefficients, respectively. The surface ocean waters in the subtropical regions due to intense evaporation $F_s/2$ have high salinity S_e, however the high water temperature T_e maintains the low density and prevent surface waters sinking.

In high latitude areas, the formation of dense water is mainly associated with lower temperatures T_p and increased salinity S_p due to the formation of ice. Thus, in the polar regions, the increase in surface water density causes it to sink and displace

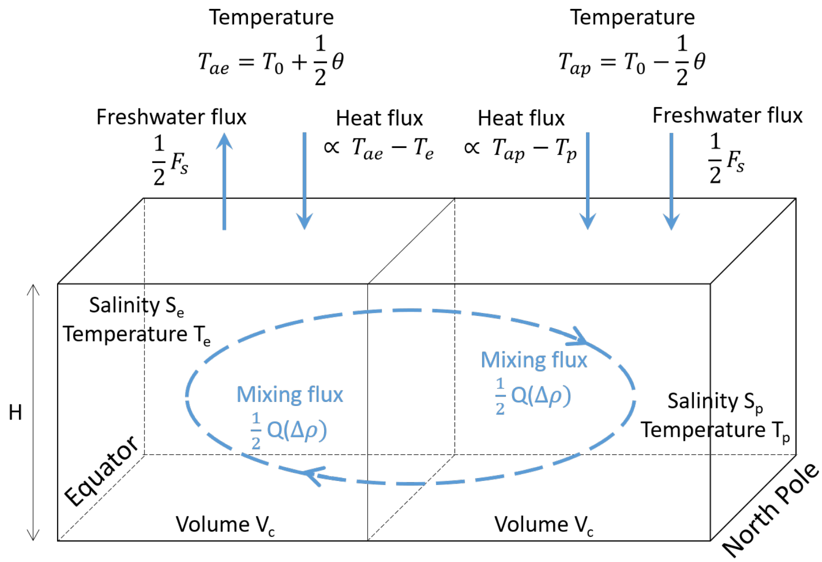

Figure 1. The two-compartment model of Stommel adapted from (Cessi, 1994). Each compartment represents the waters of the equatorial and polar oceans with the same volumes $V_c = 300 \times 4.5 \times 8,250$ km^3 and temperature T_e/T_p and salinity S_e/S_p characteristic of each of them. The other system parameters are the mean ocean depth $H = 4500$ m, the exchange mass function Q, the density gradient $\Delta\rho$, the freshwater flux F_s, the equatorial atmospheric temperature T_{ae}, the polar atmospheric temperature T_{ap}, the reference temperature $T_0 = 5^o$ C, the reference salinity $S_0 = 35$ psu, the meridional temperature difference $\theta = 25$ K and the temperature relaxation time scale $t_r = 25$ days.

deep water. In this way, the origin of the thermohaline circulation is a vertical flow of surface water $\frac{1}{2}Q(\Delta\rho)$, diving to an intermediate depth or close to the bottom, depending on the density of that water. The systems of superficial and deep circulation of the oceans are interconnected. The continuation is a horizontal flow: the recently sunk waters repel in the horizontal direction the deep waters that occupied this place. In this way, the cold, dense waters sink and slowly flow towards the equator. Thermal energy and salinity balances can be defined by the system of differential equations (Cessi, 1994) (the dots represent derivative with respect to time):

$$
\begin{aligned}
\dot{T}_e &= -{t_r}^{-1}(T_e - (T_0 + \frac{\theta}{2})) - \frac{1}{2}Q(\Delta\rho)(T_e - T_p),\\
\dot{T}_p &= -{t_r}^{-1}(T_p - (T_0 - \frac{\theta}{2})) - \frac{1}{2}Q(\Delta\rho)(T_p - T_e),\\
\dot{S}_e &= \frac{F_S}{2H}S_0 - \frac{1}{2}Q(\Delta\rho)(S_e - S_p),\\
\dot{S}_p &= -\frac{F_S}{2H}S_0 - \frac{1}{2}Q(\Delta\rho)(S_p - S_e),
\end{aligned}
\tag{3}
$$

where $Q(\Delta\rho) = t_d^{-1} + V_c^{-1} q(\Delta\rho)^2$ is the exchange mass function with diffusive time scale $t_d = 180$ years between the two compartments and transport coefficient $q = 1.92 \times 10^{12}$ $\mathrm{m^3 s^{-1}}$. The other parameters of the system are defined in the caption of Fig. 1.

The time evolution of temperature $\Delta T \equiv T_e - T_p$ and salinity difference $\Delta S \equiv S_e - S_p$ between the compartments are obtained by subtracting the conservation equations (3), respectively.

$$\frac{d\Delta T}{dt} = -{t_r}^{-1}(\Delta T - \theta) - Q(\Delta\rho)\Delta T,$$
$$\frac{d\Delta S}{dt} = \frac{F_S}{H} S_0 - Q(\Delta\rho)\Delta S. \tag{4}$$

The original system (4) with the substitutions $x \equiv \frac{\Delta T}{\theta}$, $y \equiv \frac{\Delta S \beta_s}{\theta \beta_T}$, $\tau \equiv \frac{t}{t_d}$ is reduced to the dimensionless system of evolution equations (Cessi, 1994; Tesfay et. al., 2020)

$$dx = (-\beta(x-1) - x[1 + \mu^2 (x-y)^2])d\tau,$$
$$dy = (F - y[1 + \mu^2 (x-y)^2])d\tau, \tag{5}$$

where β a ratio of a diffusive and a restoring time scale, μ^2 strength of the buoyancy-driven convection between the two compartments relative to the diffusive mixing and F dimensionless fresh-water forcing are defined as

$$\beta = \frac{t_d}{t_r}, \qquad \mu^2 = \frac{q t_d (\beta_T \theta)^2}{V}, \qquad F = \frac{\beta_S S_0 t_d}{\beta_T \theta H} F_S. \tag{6}$$

The dynamical system (5) can be further simplified, since the diffusion time scale t_d is much larger than the temperature-restoring time scale t_r. Thus, taking the approximation $x = 1 + \mathcal{O}(\beta^{-1})$, we get the first order differential equation in $y(t)$

$$dy = (F - y[1 + \mu^2 (1-y)^2])dt. \tag{7}$$

where τ is replaced by the usual notation of time t for convenience. Considering that F is constant, Eq. (7) can be written as $dy = -V'(y)dt$ with the potential function

$$V(y) = \mu^2 (\frac{y^4}{4} - \frac{2}{3} y^3 + \frac{y^2}{2}) + \frac{y^2}{2} - Fy. \tag{8}$$

The variation in the fresh-water forcing strength F, Fig 2 (b), suddenly changes the qualitative behaviour of the AMOC system giving rise to the two bifurcation points $F = 0.9556$ and $F = 1.2963$. For $F < 0.9556$ the system has a single stable equilibrium point, called *on*-state, Fig 2 (a). In this state y is small and this matches with relatively large equator to north pole heat transport. For $0.9556 < F < 1.2963$, Fig 2 (d), (e) and (f) in addition to the stable *on*-state, two more equilibria emerge: one of which is stable, called *off*-state and the other is unstable one. In the *off*-state y is large and corresponds to weak (or even reversed) circulation. Only stable *off*-state takes place in the AMOC systems with $F > 1.2963$, Fig 2 (c). With global warming, by the end of the twenty-first century, the mean surface air temperature due to harmful human activities leading to the accumulation of greenhouse gases in the atmosphere will increase by $2-6^o$ C (Chapman and Shackleton, 1999; Ganachaud and

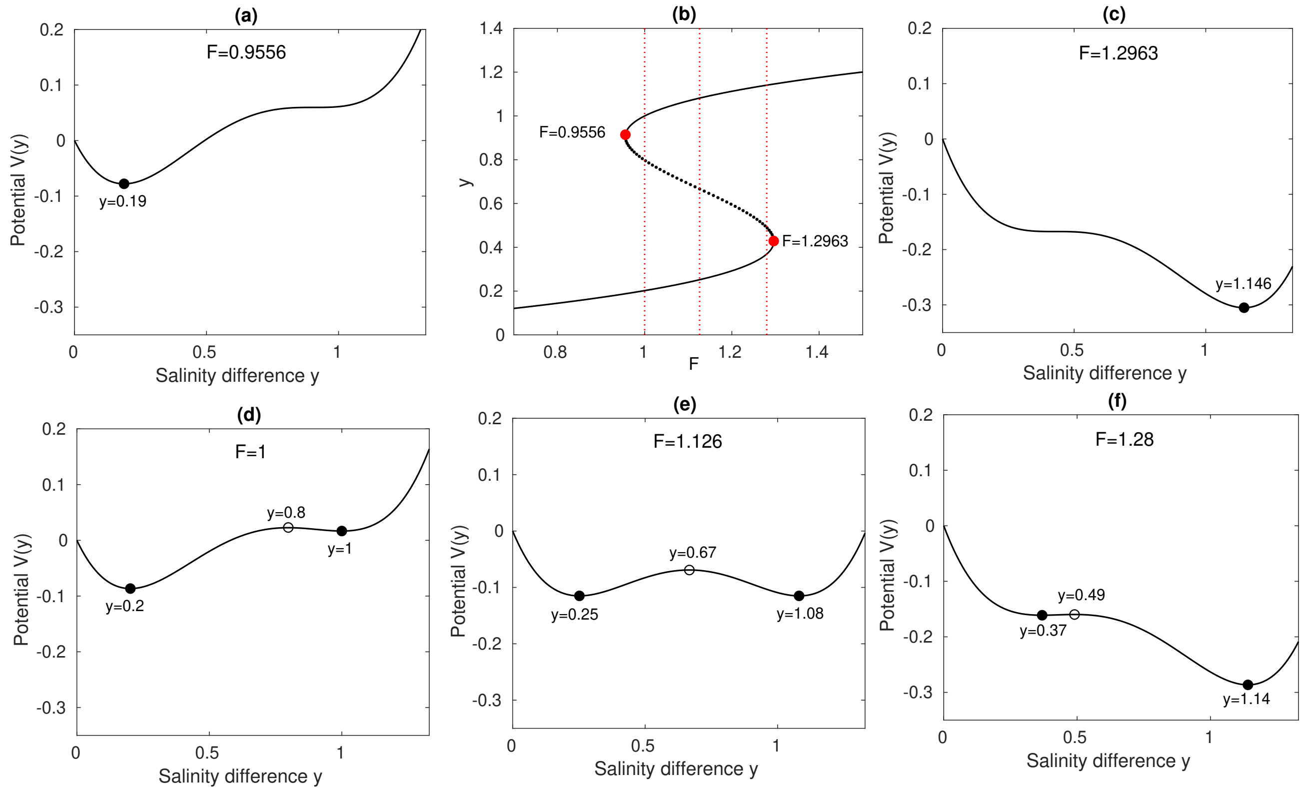

Figure 2. The Stommel two-compartment model for the meridional overturning circulation may have multiple equilibria. (b) The bifurcation diagram for the salinity difference y, as a function of fresh-water forcing strength F. The potential function $V(y)$ for forcing strength (a) $F = 0.9556$, (c) $F = 1.2963$, (d) $F = 1$, (e) $F = 1.126$ and (f) $F = 1.28$.

Wunsch, 2001; Rahmstorf, 2003). This large-scale warming of the climate can cause an increase in frequency or/and intensity of extreme events on the time-scale of decades, such as high-latitude precipitations, the Greenland ice sheet deglaciation, the freshwater outflows to the oceans that certainly affect the dynamic aspects of thermohaline circulation (Clark et. al., 2002; Jackson and Wood, 2017; Gregory et. al., 2017). An increase in the mass of freshwater in the global ocean reduces its density and thereby complicates its deep immersion, which can slow down AMOC and even "switch it off" if the parameters cross the tipping threshold (Stommel, 1961). Such extreme and fast events cannot be modeled by deterministic models, since they do not take into account the uncertainty, unpredictability and the likelihood of their occurrence. The Brownian motion predicts the behavior of such random fluctuation with very low accuracy, since it has continuous sample paths and normally distributed increments. It was proved (Ditlevsen, 1999; Marotzke, 2000) that the Lévy process, characterized by heavy-tailed distribution and discontinuous cadlag paths, with a certain precision simulates and predicts these rare events. Consider now that the freshwater flux can be written as sum of a stochastic component dL_t^α with a parameter F which is independent of time; then (7) generalizes into the Itô equation,

$$dY_t = -V'(Y_t)dt + dL_t^\alpha, \quad Y_0 = y_0. \tag{9}$$

Here L_t^α is a symmetric α-stable Lévy process, with $\alpha \in (0,2)$, defined on the probability space $(\Omega, \mathcal{F}, P)$ (See subsection 3.1). The drift term $V'(Y_t)$ satisfies a Lipschitz condition with jump measures, then the solution of the SDE (9) exists and is unique (Applebaum, 2004). We focus our attention on the three AMOC models with different values of the parameter F; a weak F=1, fresh-water forcing F=1.126 which induces a symmetric potential function and a strong F=1.28. These values represent different geometries of a double-well potential function as in Fig. 2 (d), (e) and (f).

3 Method

This section summarizes definitions and the main properties of the stability measures used in the present analysis. Also a brief summary to the type of stochastic process chosen to model extreme events is given.

3.1 A symmetric α-stable scalar Lévy motion

Climate extreme events show random fluctuations having sample pathways with intermittent jumps and heavy tails. Natural and more appropriate candidate for modeling such a non-Gaussian process is an α-stable Lévy motion. L_t^α with $0 < \alpha < 2$ is a stochastic process that satisfies the following properties:

a) $L_0^\alpha = 0$, almost sure;

b) L_t^α has independent increments;

c) stationary increments $L_t^\alpha - L_s^\alpha$ and L_{t-s}^α have the same symmetric α-stable distribution, i.e. $S_\alpha((t-s)^{\frac{1}{\alpha}}, 0, 0)$;

d) stochastically continuous sample paths, i.e., for every $s > 0$, $L_t^\alpha \to L_s^\alpha$ in probability, as $t \to s$.

The probability density function for L_t^α is defined by

$$t^{-\frac{1}{\alpha}} f_\alpha(t^{-\frac{1}{\alpha}} y), \tag{10}$$

where f_α is the probability density function for the standard symmetric α-stable random variable $Y \sim S_\alpha(1,0,0)$ (for more details see (Applebaum, 2004; Duan, 2015). The generating triplet of L_t^α is $(0, 0, \nu_\alpha)$, with the jump measure, i.e. the expected value of the number of jumps of size dz during the unit time, is defined as:

$$\nu_\alpha(dz) = \frac{\alpha\, \Gamma((1+\alpha)/2)\, dz}{2^{1-\alpha}\sqrt{\pi}\, \Gamma(1-\alpha/2)\, |z|^{1+\alpha}}, \quad \alpha \in (0,2), \tag{11}$$

where Γ is the Gamma function. When $\alpha \in (0,1)$, the α-stable Lévy motion has finite variation, otherwise, when $\alpha \in [1,2)$ it is unbounded.

Comparing two stochastic processes such as Brownian motion and Lévy flight, several differences and some similarities can be distinguished. This comparison will once again justify our choice of noise for simulating climate extreme events.

Both processes are a random walk with independent and stationary increments. Brownian motion increments have a Normal distribution, while Lévy flight step-lengths have a Lévy distribution, a probability distribution that is heavy-tailed. The sample path of the Brownian motion is continuous, differing in this from Lévy flight since its path is a cadlag function. Namely, Lévy path at most has a countable number of jumps, which are the only discontinuities in time.

3.2 Mean first exit time

The first exit time for a solution orbit from a deterministic domain $D \subset \mathbb{R}^1$ of attraction of $y_{(on/off)}$ is defined as:

$$\tau(\omega, y) = \inf\{t \geq 0, Y_t(\omega, y) \notin D\}, \tag{12}$$

and the mean exit time or the mean residence time of the process in the *on(off)*-state domain is denoted as $u(y) \triangleq \mathbb{E}\tau(\omega, y) \geq 0$. It has been proven (Duan, 2015) that the mean exit time of the stochastic system (9) for an orbit starting at $y \in D$, satisfies the following nonlocal partial differential equation with an external boundary condition

$$\begin{aligned} Au(y) &= -1, \quad y \in D \\ u(y) &= 0, \quad y \in D^c, \end{aligned} \tag{13}$$

where A is the generator defined as

$$Au(y) = -V'(y)u'(y) + \int\limits_{\mathbb{R}^1 \setminus \{0\}} [u(y+z) - u(y) - I_{\{|z|<1\}}\, zu'(y)]\nu_\alpha(dz). \tag{14}$$

Here D^c is the complement set of D in $\mathbb{R}^1$ and $I_{\{|z|<1\}}(z)$ is the indicator function for a set $|z| < 1$, defined as

$$I_{\{|z|<1\}}(z) = \begin{cases} 1, & \text{if} \quad |z| < 1, \\ 0, & \text{if} \quad |z| \geq 1. \end{cases} \tag{15}$$

Moreover, the generator can be interpreted as $Au = \lim\limits_{t \to 0} \frac{\mathbb{E}u(y_t) - u(y_0)}{t}$, for every $u \in C^2(\mathbb{R}^1)$.

3.3 Escape probability

The likelihood that the salinity difference process Y_t exits firstly from the *on(off)*-state domain D by landing in the set $U \in D^c$ belonging to the *off(on)*-state domain is represented by

$$p(y) = \mathbb{P}\{Y_\tau(y) \in U\} \tag{16}$$

and solves the following integro-differential equation with the Balayage-Dirichlet boundary condition

$$Ap(y) = 0, \quad y \in D, \tag{17}$$

$$p(y) = \begin{cases} 1, & y \in U, \\ 0, & y \in D^c \setminus U. \end{cases}$$

We use a numerical approach adapted from Gao et. al. (2014) for solving equation (17). The simplified form of this equation

$$\begin{aligned} &\frac{d}{2}p''(x) + f(x)p'(x) - \frac{\varepsilon C_\alpha}{\alpha}\left[\frac{1}{(1+x)^\alpha} + \frac{1}{(1-x)^\alpha}\right]p(x) \\ &+\varepsilon C_\alpha \int\limits_{-1-x}^{1-x} \frac{p(x+y) - p(x)}{|y|^{1+\alpha}} dy = 0, \end{aligned} \tag{18}$$

is discretized in the $x \in (-1,1)$. $p(x) = 1$ for $x \in (1,+\infty)$ and $p(x) = 0$ for $x \in (-\infty,-1)$. The corresponding schemes for the general case can be extended easily, using central difference for derivatives and the "punched-hole" trapezoidal rule getting a discretized equation of second-order accuracy for any $0 < \alpha < 2$ and $j = -J+1, ..., -2, -1, 0, 1, 2, ..., J-1$:

$$C_h \frac{P_{j-1} - 2P_j + P_{j+1}}{h^2} + f(x_j) \frac{P_{j+1} - P_{j-1}}{2h}$$
$$-\frac{\varepsilon C_{P j}}{\alpha} [\frac{1}{(1+x_j)^\alpha} + \frac{1}{(1-x_j)^\alpha}] + \varepsilon C_\alpha h \sum_{k=-J-j, k \neq 0}^{J-j}{}'' \frac{P_{j+k} - P_j}{|x_k|^{1+\alpha}} = 0 \tag{19}$$

where P_j is the numerical solution of p at x_j. The interval $[-2,2]$ is divided into $4J$ subintervals and $x_j = jh$ for $-2J \leq j \leq 2J$ integers, where $h = 1/J$. The modified summation symbol $\sum''$ means that the quantities corresponding to the two end summation indices are multiplied by $1/2$. For more information see Gao et. al. (2014).

3.4 Fokker-Planck equation

The evolution of the probability density function $p(y,t)$ for the solution paths Y_t of the SDE (9) is governed by a Fokker-Planck equation

$$\partial_t p(y,t) = A^* p(y,t), \quad p(y,0) = \delta(y - y_0), \tag{20}$$

with the initial condition $Y_0 = y_0$. Where A^* is the adjoint operator of A (14) in the Hilbert space $L^2(\mathbb{R}^1)$ that has the explicit form in the case of a symmetric α-stable Lévy motion. Thus, the equation (20) is specified as

$$\partial_t p(y,t) = -\partial_y \left[f(y) p(y,t)\right] - \int\limits_{\mathbb{R}^1 \setminus \{0\}} \left[p(y,t) - p(y-z,t) - I_{\{|z|<1\}}\, z\, \partial_y p(y,t)\right] \nu_\alpha(dz), \tag{21}$$

where $f(y) = -V'$ is a vector field of the SDE (9).

Sufficient conditions for the existence and regularity of the probability density $p(y,t)$ in the Lévy processes driven SDE (9) is established under Hörmander's condition by using the Malliavin calculus with jump. For more details, See (Chen et.al., 2015; Song et. al., 2015; Zhang, 2014) and the references therein.

3.5 Stochastic basin of attraction

The Stochastic basin of attraction (SBA) is an important theoretical and practical tool that helps to describe a metastable behavior of a system (Zheng, 2016). SBA quantifies the stability of a metastable state in a dynamical system with noise perturbation in terms of size of the basin depending on the escape probability (Serdukova et. al., 2016). SBA is the collection of initial conditions of solution processes that have low (high) probability of exit (return) from (to) a neighborhood of an attractor. This geometric tool is applicable to models with small noise and noise that is a function of an order parameter.

By Definition (Serdukova et. al., 2016), in the $\mathbb{R}^1$ state space SBA of the *on(off)* equilibrium state with the open deterministic domain of attraction D is the set $B_{on(off)}(m,M) = D^c_{II} \bigcup D_I$, where $D_I = \{y \in D \mid p(y) < m\}$, $D^c_{II} = \{y \in D^c_I \mid p(y) > M\}$, $p(y)$ is the escape probability from $D(D^c_I)$ to $D^c(D_I)$ defined in (16), m is the stability level I and M is the stability level II. In this study we consider $m = 0.3$ and $M = 0.8$.

4 Results and Discussion

The stability analysis of the *off* and *on*-states in the AMOC model is based on the three main measures: escape probability, mean first exit time and stochastic basin of attraction which are frequently used in behaviour prediction of the stochastic dynamical system trajectories and whose main properties are summarized in Section 3. In this Section we discuss the results obtained and interpret them from the climatological point of view. The potential function $V(y)$ (8) for the weak fresh-water input, as shown in Fig. 3 (a), is asymmetric and has the deepest *on*-state $(y = 0.2)$ the widest 0.8 stability basin. The length of the deterministic basin of attraction for *off*-state $(y = 1)$ is 0.26 units smaller than that for *on*-state. This indicates that under

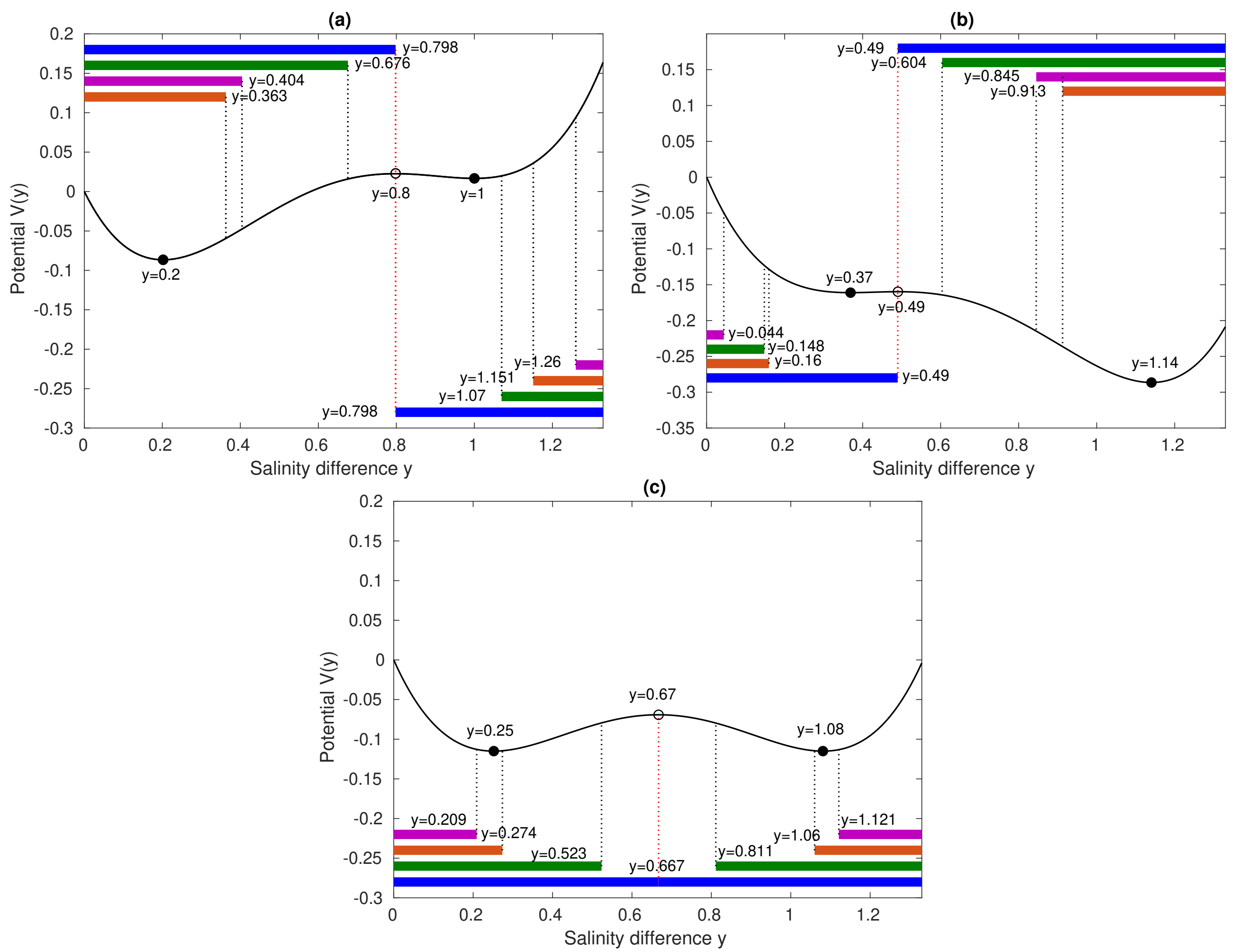

Figure 3. Stochastic basin of attraction for on(off)-metastable states of THC model, blue bar is a deterministic basin, green bar for $\alpha = 0.5$, violet bar for $\alpha = 1$ and orange bar for $\alpha = 1.5$. (a) $B_{0.2}(0.3, 0.8)$ and $B_1(0.3, 0.8)$ for $V(y)$ with $F = 1$; (b) $B_{0.37}(0.3, 0.8)$ and $B_{1.14}(0.3, 0.8)$ for $V(y)$ with $F = 1.28$ and (c) $B_{0.25}(0.3, 0.8)$ and $B_{1.08}(0.3, 0.8)$ for $V(y)$ with $F = 1.126$.

the Lévy perturbations the transition from *off*-state to *on*-state is more likely. In fact, the *off*-state basin under the noise with $\alpha = 1$ decreases by 6.75 times, while the *on*-state basin reduces only by 1.98. The greatest threat to the stability of *on*-state represents noise with low jumps of higher frequency, i.e. $\alpha = 1.5$. Extreme events of short time-scale (decades or less) such as human-induced greenhouse gas emission are more likely to destabilize the *on*-state. As a response to increase in greenhouse gas concentration, atmospheric water cycle boost is expected. This leads to a greater excess of precipitation over evaporation in high latitudes, freshening and reducing the density of surface water, and hence its tendency to sink and weaken the AMOC. The *off*-state stability, on the other hand, is more vulnerable to the perturbations with moderate jumps and frequencies, i.e $\alpha = 1$. This type of variability in the fresh-water forcing must be taken into account in the AMOC recovery programs.

The analysis of the trajectories' first mean exit time (12) and (13) from the deterministic basin Fig. 4(a) confirms the stability results based on the SBA.

Actually, the trajectories remain longer in the vicinity of *on*-state than in the *off*-state basin as the stability index (that is, α) increases. The relationship between the residence time and stability index can be understood as the extreme event modeled by

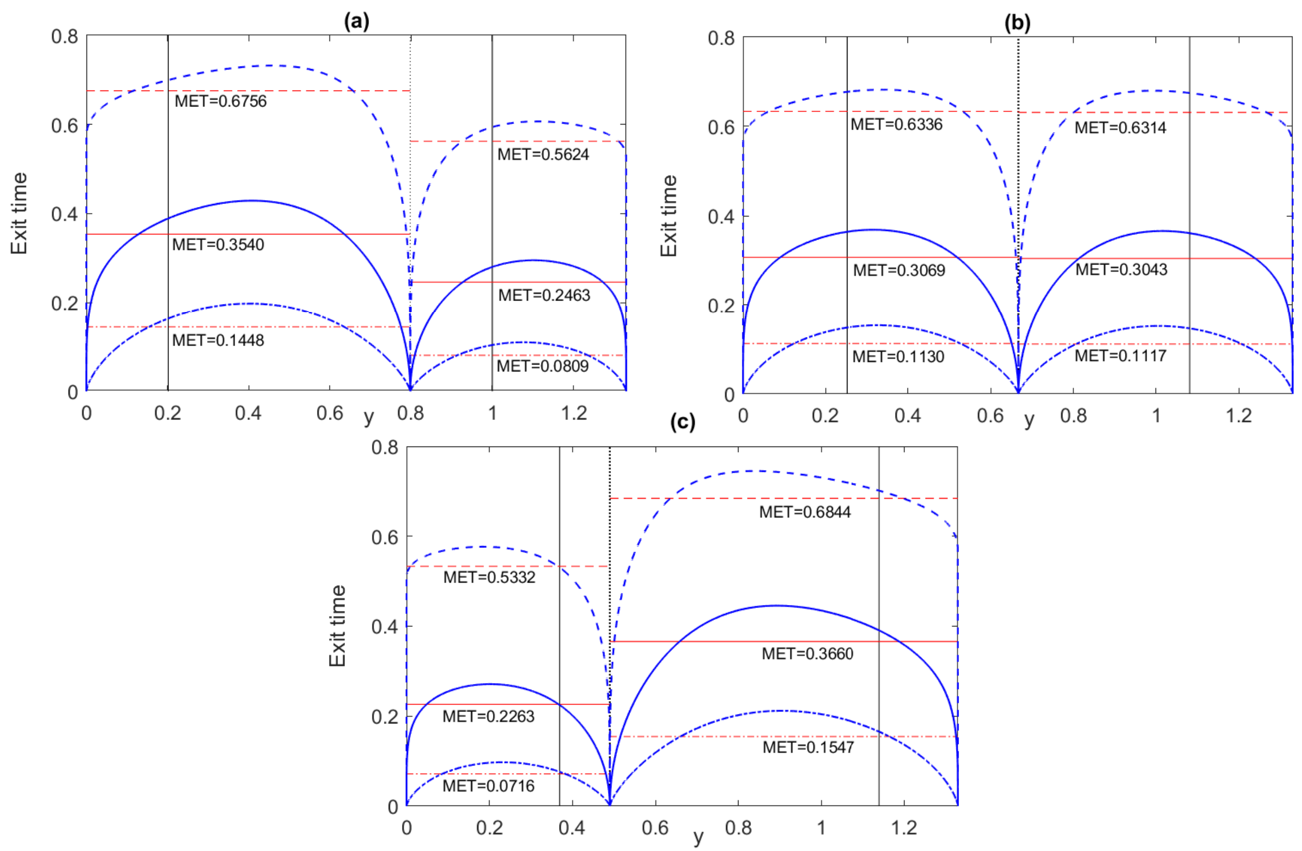

Figure 4. First exit time and mean first exit time MET of orbits with $\alpha = 0.5$ (dashed line), $\alpha = 1$ (solid line), $\alpha = 1.5$ (dash-dotted line) from the respective deterministic basins for (a) the potential $V(y)$ with $F = 1$; (b) the potential $V(y)$ with $F = 1.126$; (c) the potential $V(y)$ with $F = 1.28$.

Lévy motion with small jumps and high frequency ($\alpha = 1.5$) contributes to faster escape compared to the events characterized by moderate or big jumps that correspond to moderate or low probability ($\alpha = 1$ or 0.5). Actually, when rate of fresh-water released is large (Jackson and Wood, 2017) the timescale of AMOC weakening is measured in decades and does not depend on the actual rate of fresh-water inflow, because advective feedbacks become enhanced.

For strong fresh-water forcing the potential function $V(y)$ is also asymmetric, but now with the reversed depth: *off*-state $y = 1.14$ here is deeper than *on*-state $y = 0.37$. In this model Fig. 3 (b), *off*-state is more stable than *on*-state and this implies that under the influence of stochastic noise, the transitions from *on* to *off* are more expected.

Comparing the dimension of the effects that noise with different α parameter values causes in the meridional overturning circulation, it should be noted that the extreme events modeled by Lévy motion with $\alpha = 0.5$ does not reduce the stability of the *off*-state significantly, inducing only 0.114 unit cutback in the basin width. The noise with the short jumps and the high frequency destabilizes the *off*-state more than the extreme events with moderate jumps and frequency. The long-term stability (450-year duration of the model integration) of AMOC *off*-state was also revealed in the study of eddy-permitting climate model (Mecking et. al., 2016) and explained by the combination of the anomalous northward freshwater transport with the freshening due to reduced evaporation in this region.

In the case of the *on*-state stability, noise with the same parameter $\alpha = 1$ induces the greatest eleven times shrink of its deterministic basin. Simulation results in Fig. 5 (c) indicate the noise-driven orbits escape faster from the *on*-state and stay longer in the *off*-state basin.

The symmetry in the potential $V(y)$ is presented for $F = 1.126$ (see Fig. 3 (c)) generating the equality of the lengths of the *on(off)*-states stability basins. Also, under the force of stochastic noise, the transition from one state to another is equiprobable. The greatest destabilizer of the states is the perturbation with moderate jumps and high probability, alternatively the events characterized by low probability but high jumps bring less transient impact between the states. In Fig 4 (b), the mean exit time of the orbits from the neighborhoods of *on(off)*-states is the same and manifests the highest values for the orbits carried by Lévy noise with $\alpha = 0.5$. This shows as well that such type of perturbations has minimal influence on the stability of the states.

In Fig. 5 the D_I and D_{II}^C SBA criteria (Serdukova et. al., 2016) based on the escape probabilities (16) and (17) for the stable *on(off)*-states of the AMOC model with different fresh-water forcing F are shown: (a)-(d) for weak fresh-water input, (e)-(h) for symmetric potential well inducing fresh-water input and (i)-(l) for strong forcing. The first criteria defines the set D_I of the initial salinity difference y_0 that originate the trajectories with the $m < 0.3$ probability of escape from the deterministic basin of *on*-state Fig. 5 (a), (e), (i) and *off*-state (d), (h), (l). The trajectories with probability $M > 0.8$ of return to the interval D_I have their initial points y_0 included by the second criteria in the *on*-state's SBA Fig. 5 (b), (f), (j) (*off*-state's SBA (c), (g), (k)). The geometry of the probability density functions (20) and (21) of the salinity difference process Y_t Fig. 6, once again confirms the previous conclusions about the stability of the *on(off)*-states. Therefore, the process is most likely to remain in the state that represents the deepest valley in the potential function $V(y)$, this is in *on*-state for weak forcing and in *off*-state for strong forcing. For symmetrical potential well inducing forcing, the orbits with equal probability visit *on* or *off*-states. The transition between the states is more likely if the AMOC system undergoes to Lévy perturbations with low jumps and high noise probability as shown in Fig. 6 (c), since the difference between the probabilities of staying in each of the states is smaller.

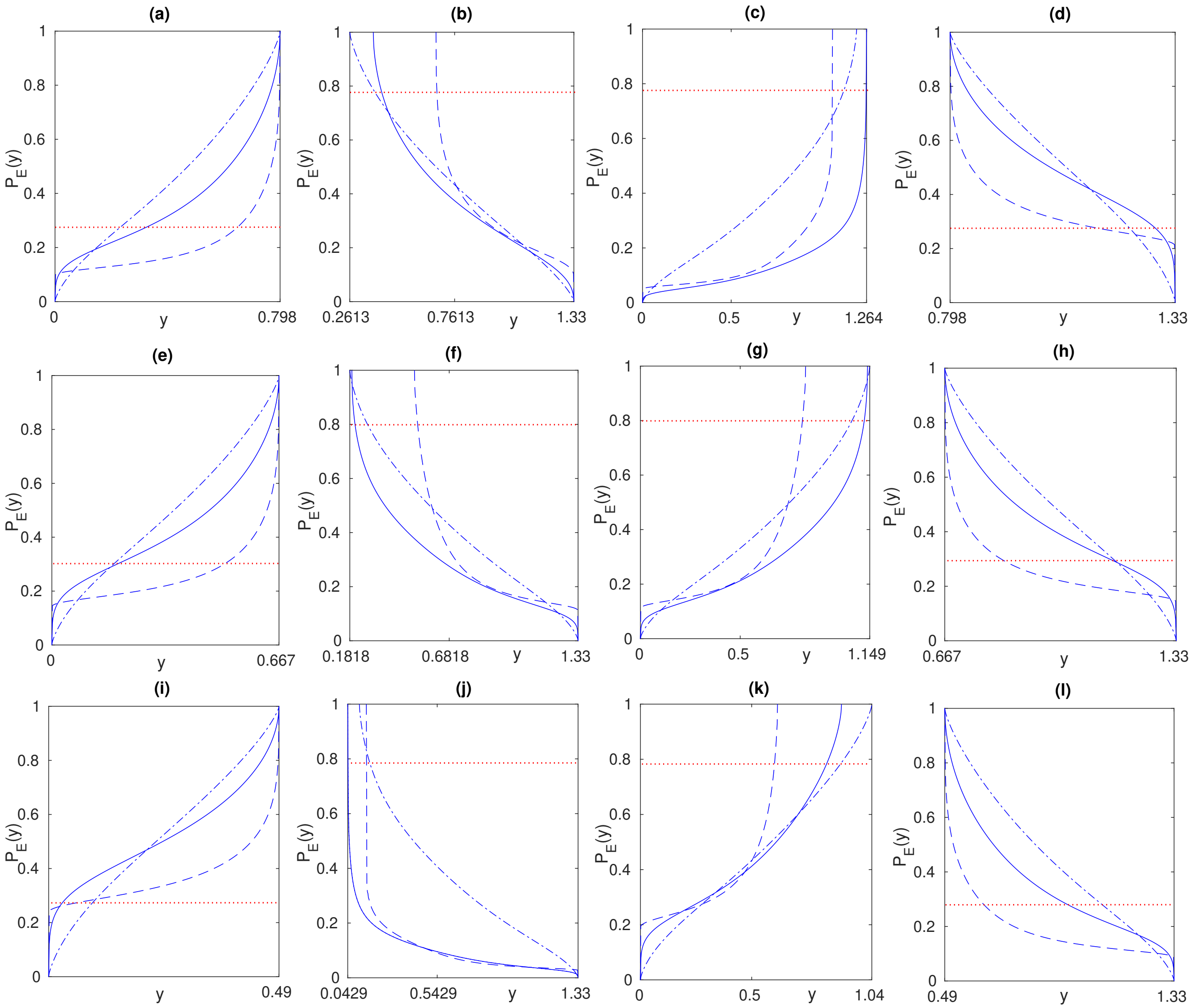

Figure 5. Escape probability of solutions with $\alpha = 0.5$ (dashed line), $\alpha = 1$ (solid line), $\alpha = 1.5$ (dash-dotted line) (a) from $D = (0, 0.798)$ to $D^c = (0.798, 1.33)$; (b) from $D_I^c = (0.6723, 1.33)/(0.3731, 1.33)/(0.2613, 1.33)$ to $D_I = (0, 0.6723)/(0, 0.3731)/(0, 0.2613)$ for the respective α; (c) from $D = (0.798, 1.33)$ to $D^c = (0, 0.798)$; (d) from $D_I^c = (0, 1.072)/(0, 1.264)/(0, 1.208)$ to $D_I = (1.072, 1.33)/(1.264, 1.33)/(1.208, 1.33)$; (e) from $D = (0, 0.667)$ to $D^c = (0.667, 1.33)$; (f) from $D_I^c = (0.5069, 1.33)/(0.1918, 1.33)/(0.1818, 1.33)$ to $D_I = (0, 0.5069)/(0, 0.1918)/(0, 0.1818)$; (g) from $D = (0.667, 1.33)$ to $D^c = (0, 0.667)$; (h) from $D_I^c = (0, 0.8278)/(0, 1.138)/(0, 1.149)$ to $D_I = (0.8278, 1.33)/(1.138, 1.33)/(1.149, 1.33)$; (i) from $D = (0, 0.490)$ to $D^c = (0.490, 1.33)$; (j) from $D_I^c = (0.147, 1.33)/(0.04287, 1.33)/(0.1078, 1.33)$ to $D_I = (0, 0.147)/(0, 0.04287)/(0, 0.1078)$; (k) from $D = (0.49, 1.33)$ to $D^c = (0, 0.49)$; (l) from $D_I^c = (0, 0.616)/(0, 0.9037)/(0, 1.04)$ to $D_I = (0.616, 1.33)/(0.9037, 1.33)/(1.04, 1.33)$. (a)-(d) The potential function $V(y)$ for forcing strength $F = 1$; (e)-(h) The potential function $V(y)$ for forcing strength $F = 1.126$ (i)-(l) The potential function $V(y)$ for forcing strength $F = 1.28$. Red dotted lines $P_E(y) = 0.3$ and $P_E(y) = 0.8$ are parameters m and M.

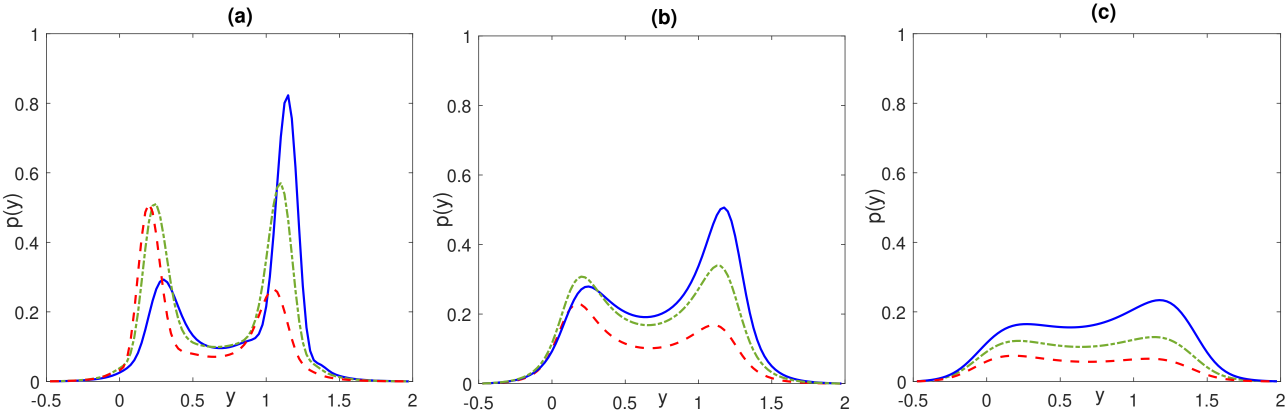

Figure 6. Probability density function $p(y,t)$ for the salinity difference process Y_t with initial condition $Y_0 = y_0$, $t = 50$, $p(y,0) = \delta(y - y_0)$ for the potential $V(y)$ with $F = 1$ dashed orange line $y_0 = 0.8$, with $F = 1.126$ dash-dotted green line $y_0 = 0.67$, with $F = 1.28$ solid blue line $y_0 = 0.49$ and (a) $\alpha = 0.5$; (b) $\alpha = 1$; (c) $\alpha = 1.5$.

Therefore, for $\alpha = 0.5$ Fig. 6 (a) the probability that the process remains in *off*-state is 2.87 times greater than in *on*-state. This difference in probabilities decreases with the increase in α parameter (which means a decrease in height and an increase in the frequency of jumps), resulting in a difference of 1.81 times for $\alpha = 1$ Fig. 6 (b) and 1.42 times for $\alpha = 1.5$ Fig. 6 (c).

5 Conclusion

Fluctuations in the AMOC patterns influence climate, in its turn civilization-induced and natural climatic changes have impacts on AMOC. The meridional overturning circulation is bistable only for some domain of the nondimensional fresh-water parameter values. Extreme events such as greenhouse gas emissions, collapse of major ice sheets and global warming induce a transition between both states. It has, therefore, great importance to sufficiently scrutinize the stability of strong (weak) AMOC states against these extreme events. In this work, we have performed analysis of stability of the *on*-state and *off*-state in the stochastic two-compartment Atlantic meridional overturning circulation model by considering three different values of the fresh-water input control parameter.

Random noise agitations in geophysical complex dynamical systems have been regarded as continuous perturbation or Gaussian processes. However, the paleoclimatic data sets signify random fluctuations in swift climatic transitions have a non-Gaussian distribution with heavy tail and pathways that are cádlág functions with at most a countable number of jumps. Therefore, it is more fitting applying non-Gaussian symmetric α-stable Lévy processes in modeling the influence of extreme events in the conceptual stochastic Stommel two-compartment model. Actually, these non-Gaussian processes are becoming increasingly popular lately.

We applied three concepts, mean residence time, first passage probability and stochastic basin of attraction. Each of these quantities is helpful in understanding the stability of the strong AMOC (small salinity difference y) state and the weak AMOC (large salinity difference y) against stochastic perturbations (extreme events) and predicting transitions between these states.

The main conclusion of our work are the following: For the weak fresh-water flux, *on* to *off*-state transition is more probable under extreme events modeled by Lévy noise perturbations with smaller jumps but with high frequency. This SBA analysis result is confirmed by calculating MET of sample paths. In the deterministic case, *on*-state has the widest basin of attraction as compared to both symmetric well potential inducing and strong fresh-water influxes. Our results for strong fresh-water input indicate extreme events of moderate jumps and frequencies facilitate the recovery of the strong AMOC, i.e., the transition from *off* to *on*-state is boosted. Strong AMOC state attraction basin suffers its largest shrink to extreme events with a moderate jump and probability Lévy noise and noise-driven pathways linger in the attraction basin of the weak AMOC state. Both strong and weak AMOC state have equal basin stability and transitions between the states are equiprobable for the symmetric potential well inducing fresh-water forcing. The geometry of the probability density function also shows that pathways shuttle between both states. Extreme events characterized by medium jumps and frequency destabilize the states most, while events with smaller jumps and high frequency bring less transient impact.

Code availability. Results of calculations are available by e-mail request.

Author contributions. DT and LS performed the computations and writing. PW and YZ contributed in computing and methods. JD and JK revised the paper.

Competing interests. The authors declare that they have no conflict of interest.

Acknowledgements. This work was partly supported by the National Natural Science Foundation of China (NSFC) (Grant Nos. 11801192, 11531006, and 11771449).

References

Applebaum, D., Lévy processes and stocahstic calculus, Cambridge Studies in Advanced Mathematics, 2nd edn., Cambridge University Press, Cambridge, 2004.

Bergund, N.and Gentz, B.: Metastability in simple climate models: pathwise analysis of slowly driven Langevin equations, Stoch. Dyn., 2, 327-356, https://doi.org/10.1142/S0219493702000455, 2002.

Broecker, W.: The great ocean conveyor, Natural History Magazine, 97, 47-82 1987.

Bond, G., Showers, W., Cheseby, M., Lotti, R., Almasi, P., deMenocal, P., Priore, P., Cullen, H., Hajdas, I., and Bonani, G.: A pervasive millenial-scale cycle in North Atlantic Holocene and glacial climates, Science, 278, 1257-1265, https://doi.org/10.1126/science.278.5341.12571997, 1997.

Caesar, L., Rahmstorf, S., Robinson, A., Feulner, G., and Saba, V.: Observed fingerprint of a weakening Atlantic Ocean Overturning Circulation, Nature, 556, 191-196, https://doi.org/10.1038/s41586-018-0006-5, 2018.

Cessi, P.: A simple box model of stochastically-forced thermohaline flow, J. Phys. Oceanogr., 24, 1911-1920, https://doi.org/10.1175/1520-0485(1994)024<1911:ASBMOS>2.0.CO;2, 1994.

Chapman, M. R. and Shackleton, N. J.: Global ice-volume fluctuations, North Atlantic ice-rafting events, and deep-ocean circulation changes between 130 and 70 ka, Geology, 27, 795-798, https://doi.org/10.1130/0091-7613(1999)027<0795:GIVFNA>2.3.CO;2, 1999.

Chen, Z. Q., Song, R., and Zhang, X.: Stochastic flows for Lévy processes with Hölder drifts, arXiv preprint arXiv:1501.04758, 2015.

Clark, P. U., Pisias, N. G., Stocker, T. F., and Weaver, A. J.: The role of the thermohaline circulation in abrupt climate change, Nature, 415, 863-869, https://doi.org/10.1038/415863a, 2002.

Dijkstra, H.A., Nonlinear Climate Dynamics, Utrecht University, Cambridge University Press, New York, USA, 2013.

Djikstra, H.A. and Weijer, W.: Stability of the global ocean circulation: basic bifurcation diagrams, J. Phys. Oceanogr., 35, 933-948, https://doi.org/10.1175/JPO2726.1 , 2005.

Ditlevsen, P. D.: Observation of α-stable noise induced millennial climate changes from an ice-core record, Geophys. Res. Lett., 26, 1441-1444, https://doi.org/10.1029/1999GL900252, 1999.

Duan, J.: An Introduction to Stochastic Dynamics, Cambridge University Press, New York, USA, 2015.

Fuhrer, K., Neftel, A., Anklin, M., and Maggi, V.: Continuous measurements of hydrogen peroxide, formaldehyde, calcium and ammonium concentrations along the new GRIP ice core from Summit, Central Greenland, Atmos. Environ., 27A, 1873-1880, https://doi.org/10.1016/0960-1686(93)90292-7, 1993.

Ganachaud, A. and Wunsch, C.: Improved estimates of global ocean circulation, heat transport and mixing from hydrographic data, Nature, 408, 453-457, https://doi.org/10.1038/35044048, 2001.

Gao T, Duan J, Li X, et al: Mean exit time and escape probability for dynamical systems driven by Levy noise. SIAM J. Sci. Computing, 36, 887–906, https://doi.org/10.1137/120897262, 2014.

Gregory, J.M., Saenko, O.A., and Weaver, A.J.: The role of atlantic freshwater balance on the hysteresis of the meridional overturning circulation, Clim. Dyn., 51, 707-717, https://doi.org/10.1007/s00382-003-0359-8, 2017.

Grootes, P. M. and Stuiver, M.: 18O/16O variability in Greenland snow and ice with 103 to 105-year time resolution, J. Geophys. Res., 26, 455-470, https://doi.org/10.1029/97JC00880, 1997.

Huang, R.X., Luyten, J.R., and Stommel, H.M.: Multiple equilibrium states in combined thermal and saline circulation, J. Phys. Oceanogr., 22, 231-246, https://doi.org/10.1175/1520-0485(1992)022<0231:MESICT>2.0.CO;2, 1992.

Jackson, L. C., and Wood, R. A.: Timescales of AMOC decline in response to fresh water forcing, Clim. Dyn., 51, 1333-1350, https://doi.org/10.1007/s00382-017-3957-6, 2017.

Jackson, L. C., and Wood, R. A.: Hysteresis and Resilience of the AMOC in an Eddy-Permitting GCM, J. Phys. Research Letter, 45, 8547-8556, https://doi.org/10.1029/2018GL078104, 2018.

Kuhwald, I. and Pavlyukevich, I.: Stochastic resonance in systems driven by α-stable Lévy noise, Procedia Engineering, 144, 1307-1314, https://doi.org/10.1016/j.proeng.2016.05.129, 2016.

Marotzke, J.: Abrupt climate change and the thermohaline circulation: mechanisms and predictability, Proceedings of the National Academy of Sciences of the USA, 97, 1347-1350, https://doi.org/10.1073/pnas.97.4.1347, 2000.

Mecking, J., Drijfhout, S., Jackson, L. and Graham, T.: Stable AMOC off state in an eddy-permitting coupled climate model, Clim. Dyn., 47, 2455-2470, https://doi:10.1007/s00382-016-2975-0, 2016.

Mikolajewicz, U. and Maier-Reimer, E.: Internal secular variability in an ocean general circulation model, Clim. Dyn., 4, 145-156, https://doi.org/10.1007/BF00209518, 1990.

Rahmstorf, H.: Thermohaline circulation: the current climate, Nature, 421(6924):699, https://doi.org/10.1038/421699a, 2003.

Rahmstorf, S.: Multiple convection patterns and thermohaline flow in an idealized OGCM, J. Clim., 8, 3028-3039, https://doi.org/10.1175/1520-0442(1995)008<3028:MCPATF>2.0.CO;2, 1995.

Rahmstorf, S.: On the freshwater forcing and transport of the atlantic thermohaline circulation, Clim. Dyn., 12, 799-811, https://doi.org/10.1007/s003820050144, 1996.

Serdukova, L., Zheng, Y., Duan, J., and Kurths, J.: Stochastic basins of attraction for metastable states, Chaos, 26, 073117, https://doi.org/10.1063/1.4959146, 2016.

Sgubin, G., Swingedouw, D., Drijfhout, S., Mary, Y. and Bennabi, A.: Abrupt cooling over the North Atlantic in modern climate models, Nature Communications, 8, 14375, https://doi:10.1038/ncomms14375, 2017.

Song, Y., Zhang, X.: Regularity of density for SDEs driven by degenerate Lévy noises, Electronic Journal of Probability, 20, https://doi.org/10.1214/EJP.v20-3287, 2015.

Stommel, H.: Thermohaline convection with two stable regimes of flow, Tellus, 13, 224-230, https://doi.org/10.1111/j.2153-3490.1961.tb00079.x, 1961.

Tesfay, D., Wei, P., Zheng, Y., Duan, J., and Kurths, J.: Transitions between metastable states in a simplified model for the thermohaline circulation under random fluctuations, Appl. Math. Comput., 369, https://doi.org/10.1016/j.amc.2019.124868, 2020.

Timmermann, A., Gildor, H., Schulz, M., and Tziperman, E.: Coherent resonant millennial-scale climate oscillations triggered by massive meltwater pulses, J. Clim., 21, 2569-2585, https://doi.org/10.1175/1520-0442(2003)016<2569:CRMCOT>2.0.CO;2, 2003.

Trenberth, K.E. and Solomon, A.: The global heat balance: heat transports in the atmosphere and ocean, Clim. Dyn., 10, 107-134, https://doi.org/10.1007/BF00210625, 1994.

Vélez-Belchí, P., Alvarez, A., Colet, P., and Tintoré, J.: Stochastic resonance in the thermohaline circulation, Geophys. Res. Lett., 28, 2053-2056, https://doi.org/10.1029/2000GL012091, 2001.

Zhang, X.: Densities for SDEs driven by degenerate α-stable processes, Ann. Probab., 42, 1885-1910, https://doi.org/10.1214/13-AOP900, 2014.

Zheng, Y., Serdukova, L., Duan, J. et al.: Transitions in a genetic transcriptional regulatory system under Lévy motion. Sci Rep 6, 29274, https://doi.org/10.1038/srep29274, 2016.